ELSEVIER

Journal of Alloys and Compounds 253–254 (1997) 529–541

Journal of ALLOYS AND COMPOUNDS

Kinetics and mechanisms of metal hydrides formation—a review

Joseph Bloch[a,*], Moshe H. Mintz[a,b]

[a]*Nuclear Research Center–Negev, P.O. Box 9001, Beer-Sheva 84190, Israel*
[b]*Ben-Gurion University of the Negev, Department of Nuclear Engineering, P.O. Box 653, Beer-Sheva 84105, Israel*

Abstract

The microscopic mechanisms which may control the rate of the reaction of gaseous hydrogen and hydride-forming metals are reviewed. A distinction is made between the early stages of the reaction associated with the nucleation and growth of the hydrides on the surface of the reacting metal and the subsequent massive stage. For the very early stage, factors affecting the ability of hydrogen gas to penetrate surface passivation layers are considered. Different types of nucleation groups are demonstrated. For the latter, massive stage, possible morphological forms of the hydride phase development are summarized. A special case, frequently encountered in binary metal–hydrogen systems, is the contracting envelope (or shrinking core) morphology. For this case, a simple evaluation of the reaction front velocity can be deduced from the overall rate measurements and from the known geometry and dimensions of the metal sample. A detailed analysis of this hydride-front velocity dependence on sample temperature and gas pressure can then point to the controlling mechanism. Some characteristics of Arrhenius-type curves and possible deviations from linear relation are discussed. Examples for possible surface-controlled (Ce), diffusion-controlled (Th, Ti, Zr, Hf) and interface-controlled (U) reactions are presented, as well as limited bulk intermetallic hydriding reactions. Certain symptomatic aspects of the kinetic behaviour related to some of the above mechanisms are discussed.

Keywords: Kinetics; Reaction rate; Nucleation; Growth

1. Introduction

The hydrogen–metal heterogeneous reaction proceeds by a series of elementary microscopic steps, through which hydrogen atoms are transferred from the gas phase into the solid product [1]. The purpose of a particular kinetic study is to determine the rate limiting step in this sequence [2] and to find an appropriate intrinsic kinetic parameter [3]. There are two levels of 'intrinsity' recognized in the literature: In the first level the kinetic parameter should represent the overall isothermal reaction, being independent of heat or mass flow effects [2]. In the next level, the real intrinsic kinetic parameter (IKP) is defined, uniquely characterizing the specific reacting metal (or alloy) which is not affected by factors such as shape, size and topochemistry [3]. In order to obtain a meaningful IKP, it is necessary to utilize, besides measuring of the overall reaction rate, metallographic examinations of in situ hydriding processes or of partially reacted samples. It is also required to use well-defined geometries of the reacting metals. Even under such experimental conditions, the determination of the IKPs is rather difficult.

In recent years, a considerable amount of experimental observations have been accumulated concerning the hydriding kinetics and mechanisms of metal and alloys. It is possible to use this data to demonstrate some general trends of the kinetics of metal– (and alloys)–hydrogen systems. In the present paper some of these studies are reviewed, and some common features are extracted. The review is divided into two main parts, dealing with the initial (Section 2, Section 3) and the main (Section 4) hydriding stages, respectively. The initial stages are associated with the so-called 'incubation' or 'induction' periods, usually observed with hydrogen absorption curves. Only subjects which can be experimentally demonstrated are discussed. The main purpose of the review is to compare different metal–hydrogen systems in order to obtain more insight concerning the complex metal hydriding reaction, and to point to possible research directions in this field.

2. Initial surface stages

The first steps of any metal–hydrogen reaction involve

*Corresponding author. Fax: (972-7) 554848; e-mail: bloch@bgumail.bgu.ac.il

0925-8388/97/$17.00
PII S0925-8388(96)03070-8

with the mass transport of hydrogen molecules onto the solid–gas interface, dissociation of the molecules on the surface (chemisorption), at special dissociation sites, possible migration to such sites or to entering sites, and, eventually, penetration of hydrogen atoms through the surface into the bulk. At the end of this sequence, the hydrogen atoms are dissolved in the bulk metal at the vicinity of the solid–gas interface.

The interaction of hydrogen gas with clean or oxidized metal surfaces has been extensively studied using a wide selection of surface analysis techniques [4]. However, the application of such surface studies to the hydriding mechanism is not quite simple. Most hydride-forming metals and alloys are normally covered with a surface passivation layer (SPL). This layer consists of a combination of the metal oxides, hydroxides, carbon–oxygen compounds and water. A real hydriding process is performed under relatively high pressures (typically 10^2–10^7 Pa) on surfaces covered with SPL which is not always well-defined, whereas surface studies are carried out mostly under ultra-high vacuum (UHV) (better than 10^{-8} Pa) on crystalline well-defined surfaces. A similar problem is encountered in catalysis research. The extrapolation from surface analysis to the real world is not unmistakably correct. In addition, most of the surface studies were performed on transition metals of the higher groups (especially the Ni and Cu groups). Relatively few results were obtained for the characteristic hydride-forming metal elements such as groups IIIb and IVb, the rare earths [5] and actinides. In the present article the extensive surface research of hydrogen on metals is not reviewed.

Though the initial surface steps of the hydriding reaction described above are difficult to measure directly, some important information about them has been obtained indirectly. Probably the best known examples are related to the surface activation of intermetallic compounds. Thus, the use of surface analysis has revealed the presence of metallic Ni clusters on the reactive surface of $LaNi_5$ which can serve as dissociation sites for molecular hydrogen, thus accounting for the easy activation of this compound [6]. Little more complex models have been suggested for FeTi ([4], p. 76). The important role the metal surface may play in the hydriding kinetics is further demonstrated by the enhancement of the hydrogen absorption ability of several metals which are difficult to be hydrided using a deposition of a few monolayers of Pd, Pt or Ni on their external surface. Such enhancement was found for Nb and Ta [7], V [8], Mg [9] and Zr [10]. Other surface modifications affecting the hydrogen uptake rates are ball milling of metal powders under low hydrogen pressures [11], addition of a catalytic agent (Pd) to the metal powder [12], surface treatment using chemical solution [13,14] and ion implantations [15].

While the presence of high electron affinity metals on the sample surface enhances the hydrogen absorption rate, the SPL effect is to reduce the uptake rate ([16] and [4] (p. 37)). The SPL acts as a diffusion barrier for hydrogen penetration and also affects the density of dissociation centers for H_2 molecules [17]. Increasing the thickness of the oxide layer on zirconium linearly increases the hydriding incubation times [18,19]. Inhibition of hydrogen absorption due to oxide film was also found for Ti [20]. Similarly, rates of hydride nucleation on uranium metal surface were reduced with increasing thickness of oxide film [21]. Heat treatment in vacuo may induce solution of the SPL into the bulk metal and an appearance of clean metal on the surface [22], thus enhancing the initial hydriding steps. Solution of the oxide layers in bulk metal were found for U [23,24], Ti [25] and Zr [26], as well as for Zr-containing alloy getters [27,28]. Heating the sample in vacuo to relatively low temperature before hydriding has no significant dissolving effect on the SPL, yet it may drastically reduce the incubation times. This is a degassing effect. It was detected for Ce [29] and U [24,30] around 200 °C. This low-temperature activation effect has been mainly attributed to H_2O or the hydroxyls desorption process [24].

Preventing hydrogen molecules from entering the SPL can also be achieved dynamically through the presence of gaseous impurities in the reacting hydrogen atmosphere. This is called a ‘poisoning’ effect. It has been studied for intermetallics [31,32] as well as for pure metals [33,34]. Generally, sulfur-containing gaseous compounds such as SO_2, H_2S and CH_3SH are very effective poisoning agents. Oxygen-containing gases such as O_2, CO_2 and CO [35] are also considerably strong poisons, whereas CH_4, C_2H_4 and N_2 have no measurable effect on the hydrogen absorption kinetics [36]. Though the exact mechanisms of the general poisoning effect are as yet unclear, the rate-determining step during a poisoned hydridization is probably related to the interference of the impurity gas with the hydrogen adsorption and dissociation processes.

3. Initial hydride precipitation

As the hydrogen concentration in the metal exceeds the saturation concentration a hydride phase is formed. The topochemical characteristics of the initial hydride phase development are determined by the combination of the transport and mechanical properties of the system. Most hydride-forming intermetallics are brittle. Due to the lower density of the hydride relative to the parent alloy, the hydride formation is accompanied by strain fields resulting in the cracking of the parent alloy [37]. Pure metals, on the other hand, are much more ductile. Usually, they suffer no cracking during the initial hydriding process, but it is rather the hydride phase which is fractured. Thus, for intermetallics, the initial hydride phase is nucleated at the fresh metallic surface exposed at the cracks location. For pure metals, the first hydride nuclei usually appear at the

locations of the highest hydrogen concentration and lowest activation energy for nucleation. Evidently, the surface is such a favourable location. The exact nucleation location may be related to the presence of the dissociation site [38] or to the local properties of the SPL. In addition, under certain experimental conditions, other bulk discontinuities, e.g. grain boundaries, defects, etc. can also provide such preferred conditions. In the following some experimental results illustrating each of these paths are reviewed.

3.1. Hydride formation in brittle alloys and intermetallics

Most of the kinetic studies of intermetallics hydriding are confined to activated powdered materials [39]. The activated material consists of relatively small particles with metallic (nonoxidized) surfaces. The analysis of such kinetic data is usually difficult due to uncontrolled heat transfer [40,41]. Even for optimal isothermal experiments there are certain questions addressed to the data analysis procedure applied for powders [42]. In the present review we are interested mostly in the hydriding of bulk massive alloys, namely, in the first activation cycle [43]. Only a few studies have been performed on the initial stages of the hydriding of bulk intermetallics. Upon exposure to hydrogen the massive alloy is cracked and eventually disintegrates into small particles [44,45]. A useful technique applied to this process is the detection of the acoustic emission during the hydriding [45–47]. It seems that the appearance of visually observed macrocracks is preceded by a stage of microcracking detected by the acoustic emission [45]. The macrocracks may follow preferred paths of advance [48]. Microcracks branch from the primary cracks.

Fig. 1 shows the development of microcracks on the surface of $LaNi_{4.75}Al_{0.25}$ at room temperature and under 0.1 MPa H_2 [49]. It can be seen that microcracks are branched from primary cracks. It is also found that the cracks intend to create closed loops which eventually result in the formation of thin flakes or particles falling off the sample.

It should be emphasized again that, so far, insufficient information is available in this subject area, probably due to the difficulties in the direct measurements of initial hydriding kinetics of non-activated massive intermetallics.

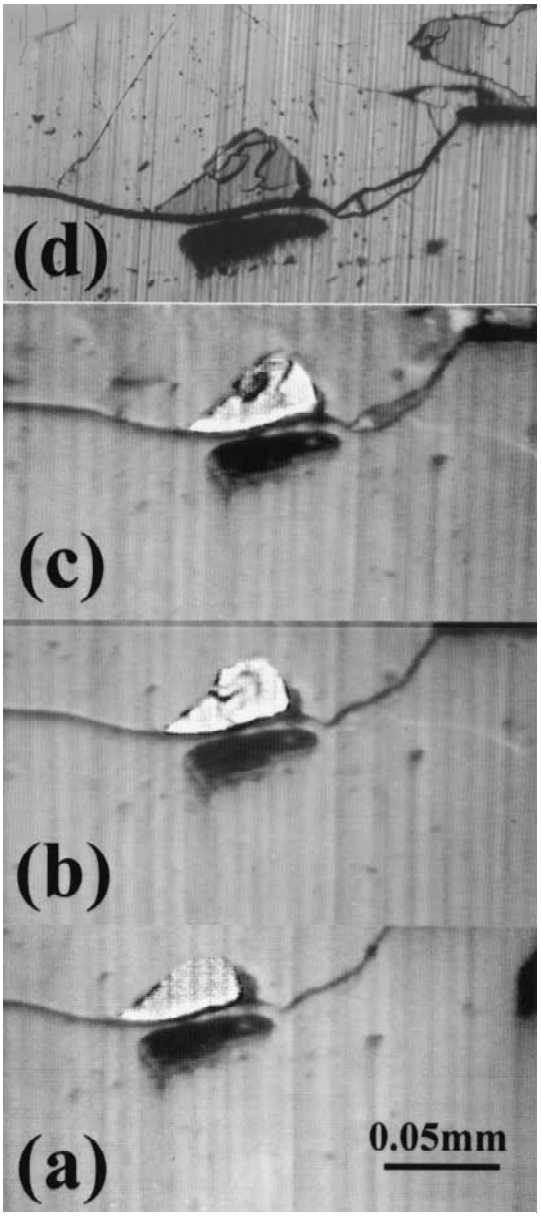

Fig. 1. Hot stage microscopy showing the development of microcracks on the surface of $LaNi_{4.75}Al_{0.25}$ at room temperature and under 0.1 MPa H_2 [49]. (a) The unhydrided sample surface; (b) 12 min exposure, a flake is formed attached to a primary crack; (c) 1 h exposure, additional cracks emerge from the primary and secondary cracks; (d) The sample after removing from the chamber, photographed by a separate microscope to obtain better resolution.

3.2. Surface hydride nucleation and growth

For pure metals, hydride precipitation which initiates at the surface does not induce the cracking and particulation of the sample at this early stage (as mentioned for the more brittle intermetallics). Hence, the nucleation and growth (NG) processes on the surface can be monitored utilizing hot stage microscopy (HSM) techniques [50].

Most of the models developed to describe overall NG kinetics were derived for experimental results based on solid-phase transformations [51] and thermal decomposition of solids [52]. In the case of hydriding reactions, models of NG were suggested for activated intermetallics [2,39,53–55]. However, the fitting of particular kinetic data to a given NG model is quite ambiguous [56]. Continuous observations of hydrides NG processes have never been made for intermetallic alloys. Also, such models involve the simultaneous convolution of both contributions of nucleation rates and growth velocities which can not be separated. Only by direct observations

can these two processes be independently evaluated. It should be noted that even though NG kinetics in solid phases have been extensively studied, direct observations of these processes are quite scarce. Evidently, such observations are restricted mostly to the surface.

Studies based on direct HSM observation of NG of hydrides were performed for pure uranium [21,57], dilute uranium alloys [33,34,50], cerium [58] and gadolinium [59]. There are several common features found for this type of surface NG processes:

1. Hydride nuclei initially precipitate below the intact SPL. As the hydride nucleus grows, the strain induced by the hydride expansion causes the fracture of the SPL, exposing a fresh hydride surface. The point at which the cracking of the SPL occurs may depend on the pressure, temperature and mechanical properties of the surface. In Fig. 2 this structure of hydride nuclei on U–0.1 wt% Cr is shown. The intact and fractured parts of the nucleus are clearly observed.
2. Several different groups (or 'families') of nuclei may grow on the metal surface. The different groups are characterized by specific nucleation and growth rates. For pure uranium metal at least two groups were found [60]. For one group the nucleation rate is relatively high whereas the growth velocity is relatively low, while the second group is characterized by a lower density of 'spots' growing faster. Each of these groups prevail at a different temperature range. There is, however, a range in which both are formed simultaneously. For gadolinium, the fast (high-density) nucleated 'family' is so dense, and the size of the nuclei is so small (around 1 μm), that it can hardly be observed during the HSM in situ experiments. In fact, they appear as a fast change of colour of the sample's surface. Only higher magnification microscopy performed ex situ after partial hydriding of the Gd sample can reveal those tiny nuclei [59]. On the other hand, for Ce, only one 'family' of nuclei was identified [58].
3. The cumulative nucleation function $N(t)$ has a characteristic S-shaped form. The measured nucleation rate dN/dt can be represented by a Gaussian curve. Fig. 3 demonstrates the nucleation rate of two 'families' growing simultaneously on uranium metal surface [60]. It should be noted that Gaussian nucleation rates are not common in thermal decomposing systems [52] in which the nucleation rate is assumed to be proportional to some power of N. The interpretation of the Gaussian dependence is probably related to some random distribution of the nuclei formation times about the time the subsurface reaches saturation of a finite number of available nucleation sites.
4. Preferred nucleation sites were identified at grain boundaries [50] or inclusions [21,61]. The number of preferred nucleation sites (for a certain type, or 'family' of nuclei), N_o, is finite. This number depends on the surface characteristics of the sample, and may differ

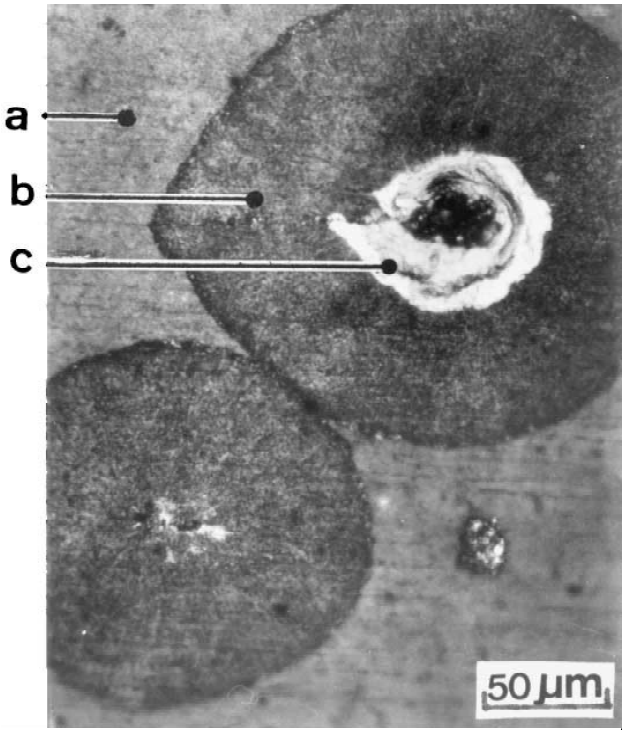

Fig. 2. Hydride nuclei developed on U–0.1 wt% Cr surface at 200 °C under 50 kPa H_2 following vacuum annealing at 400 °C for 0.5 h. (a) An unattacked region of the parent metal; (b) Adherent hydride layer formed below the SPL; (c) Fracture of the SPL at the nucleus center showing exposed fresh hydride phase.

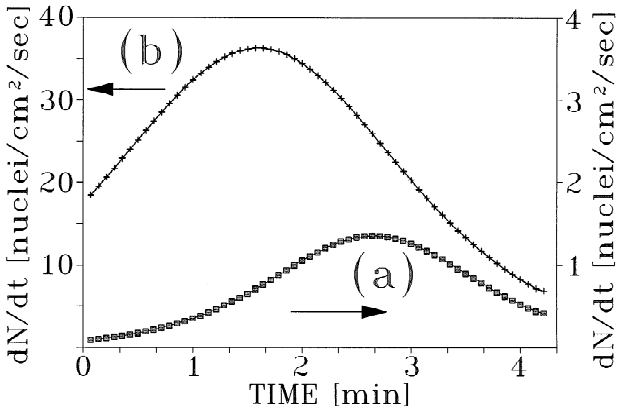

Fig. 3. Hydride nucleation rates of two group types growing simultaneously on the surface of uranium metal at 130 °C under 50 kPa H_2. The growth velocity of the slow and delayed group, (a), is much faster than that of the fast to nucleate group (b). Eventually, the sample surface is covered with hydride layer due to the growth of mainly the nuclei of group (a).

significantly for various sample preparation methods. The exact nature of these nucleation sites is not yet clear. It seems to involve a variety of parameters.

5. The geometrical shape of the growing nucleus is controlled by the extent of isotropy in the velocity of the hydride reaction front. It is evident that the bulk velocity component U_b, perpendicular to the surface may differ from the lateral velocity component, U_s, which is parallel to the surface. However, also for the lateral velocity, which is the one probed by the HSM, anisotropic growth has sometimes been observed. For nuclei growing along grain boundaries, near inclusions or in the vicinity of other heterogeneous locations, the growth rate is often both asymmetric and time dependent [62,63]. However, the growth of most nuclei is approximately isotropic producing near-circular patterns, as shown in Fig. 2. During the growth process, the reaction interface move is repeatedly interrupted. This step-like behaviour is characteristic of advance accompanied by an increasing stress-field which is periodically relieved [50,58]. Still, the average front velocity, U_s, can be obtained, characteristic of the given system under specified conditions. In Fig. 4, the growth velocities of hydride nuclei measured using HSM as a function of temperature are compared for uranium [60], gadolinium [59] and cerium [58]. In general, hydriding rates for the light rare earths (La to Nd) are faster compared with those of the heavier rare earths (Gd to Lu, excluding Yb). This is demonstrated by the higher U_s values obtained for Ce as compared with those of Gd in Fig. 4. For Gd, a break is found in the Arrhenius curve around 80 °C. This change of slope may be related to a change in the relative importance of the two 'families' of nuclei mentioned above. Thus, for uranium, where the rate of growth of the two 'families' can separately be measured, the slower rate of the fast nucleated 'family' is clearly observed.

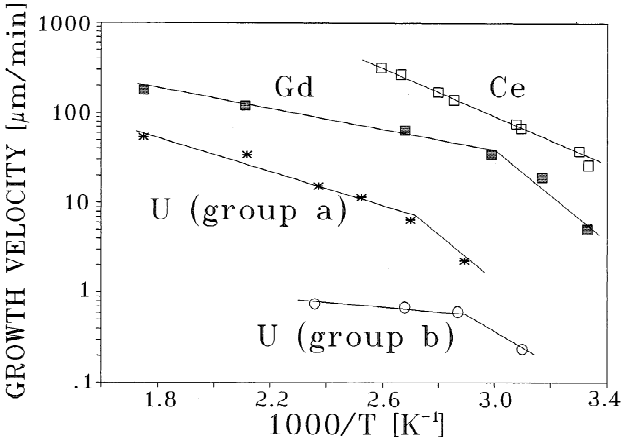

Fig. 4. The average growth velocity of hydride nuclei on the surface of several metals under 0.1 MPa H_2. For uranium, groups (a) and (b) correspond to those shown in Fig. 3, respectively.

3.3. Preferred bulk hydride nucleation and growth

It has been mentioned above that hydride nucleation follows the hydrogen concentration gradient in the metal. Normally, hydrogen accumulates just below the SPL, where nucleation usually starts (see Section 3.2). The rate at which hydrogen is accumulating under the SPL is equal to the net difference between the flux of hydrogen penetrating from the ambient through the SPL and that diffusing from the interface region into the bulk of metal [42]. Since both hydrogen diffusion rate and the hydrogen solubility in the metal phase increase exponentially with temperature, for relatively high temperatures lower gradients of hydrogen concentration are developing from the surface and into the bulk. Thus, reaching a supersaturation of hydrogen at the surface vicinity may be slowed. As a result, nucleation is preferred not only at the surface region but also along paths of higher diffusion rate and/or special regions which transform at lower saturation concentrations. One example is the grain boundary hydride development resulted from fast diffusion routes observed for certain rare earths (Tb, Dy) at high temperatures [64]. For very fast grain boundary diffusion, bulk NG can occur, at least to a certain depth [64,65]. The initial hydriding stage for annealed Zr metal is gradually changing at around 350 °C from surface to grain-boundary nucleation [66,67]. It should be noted that grain-boundary nucleation in Zr is not limited for hydrides only. It has been observed for low-pressure oxidation as well [68]. In fact, such effects of grain boundary oxidation may promote subsequent hydrogen attack through the preoxidized paths, as found for Zr [66]. Another example of anisotropic hydride nucleation resulting from unequal preoxidized paths is demonstrated by the preferred edge attack found for rare earths at certain temperature ranges [64]. This phenomenon has been accounted for by inhomogeneities in the thickness of the SPL at the edge locations. It can clarify some peculiarities found for the temperature dependence of the overall hydriding rates measured for Ce [69,29].

It is worthwhile to point that the contribution of the near-surface kinetic effects increases for higher surface-to-bulk ratios of the sample. This has been demonstrated for the hydriding of zirconium [66].

Finely powdered samples are an extreme example of a very high surface-to-bulk ratio. Hence, the hydriding mechanism for powders may be totally different to that of bulk materials. This, beside the effects of heat transfer [40,41] and distribution of particles size, shapes and reaction starting times [42], has led to significant discrepancies in the reaction rates and kinetic laws measured by different groups [2,42]. Yet, in many cases, important information about the IKPs of the hydriding reaction in

powders can be concluded from the study of bulk samples, as will be demonstrated later on.

4. The main reaction stage

4.1. The topochemical forms of hydride phase progression

4.1.1. Contracting envelope

Under certain experimental conditions, the hydride nuclei growing on the surface eventually overlap to form a continuous hydride product layer. Upon completion of this stage, the hydriding reaction kinetics is changed into the so-called 'contracting envelope' or 'shrinking core' functions [3]. The IKPs are no longer nucleation and growth parameters. Rather, it is the bulk front velocity, U_b, which becomes the kinetic parameter evaluated from the measured kinetic curves.

As pointed out [3], the development of a contracting envelope morphology is the most convenient case for the evaluation of IKPs, since, for this case, simple analytical expressions link the measured overall reaction kinetics and the front velocity, U_b. In fact, most of the rigorous kinetic studies reported in the literature are related to such contracting envelope topochemistry, and the rest of this section is focused on this case. However, it should be emphasized that besides contracting envelope progression, other more complex topochemical forms are also known. Hence, before embarking on the contracting envelope case, some examples of such forms are presented.

4.1.2. Early particulation

As mentioned in Section 3.1, in brittle intermetallic materials, hydriding is accompanied by early cracking and particulation of the sample. The hydride is repeatedly nucleated and growing on the fresh exposed surfaces. Thus, it is irrelevant to speak of the formation of a hydride front in this case. However, it is still possible that a cracked zone will move from the surface into the bulk with some effective front velocity. Such heavily cracked areas were observed near the surface of partially hydrided FeTi particles [70]. A similar cracking behaviour has been also observed for Fe Ti_{1+x} alloys [48]. For $LaNi_{0.75}Al_{0.25}$ [49] and $LaNi_5$ [56] 'dry soil' like structures were observed for partially hydrided samples. So far, no quantitative data is available for this case.

4.1.3. Grain boundary attack

Hydrogen transport and hydride nucleation are sometimes preferred along defect lines and grain boundaries (Section 3.3). This leads to the formation of hydride layers along these preferred areas. For example, for Zr metal, above the eutectoid temperature (550 °C), the hydride layer is formed internally on the circumferences of the grains. The main reaction mechanism is thus the simultaneous advance of the layer into the grains [67]. Since, in this case, each grain reacts as a single powder-like particle, the average front velocity can be calculated using powder analysis techniques [42]. Other examples for such a type of topochemical progression are given by some rare earth metals hydrided at relatively high temperatures [64].

4.2. The structure and construction of the moving hydride layer

The product-moving layer formed at the samples surface during the main reaction stage of a contracting envelope case consists of several layered regions. This is schematically described in Fig. 5a for a metal forming two types of hydrides (e.g. mono- and di-hydrides). The regions observed in the most general case are (from the inside to the outside): the parent metal, a solid-state solution of hydrogen in the α-phase [64], the lower and higher hydrides,

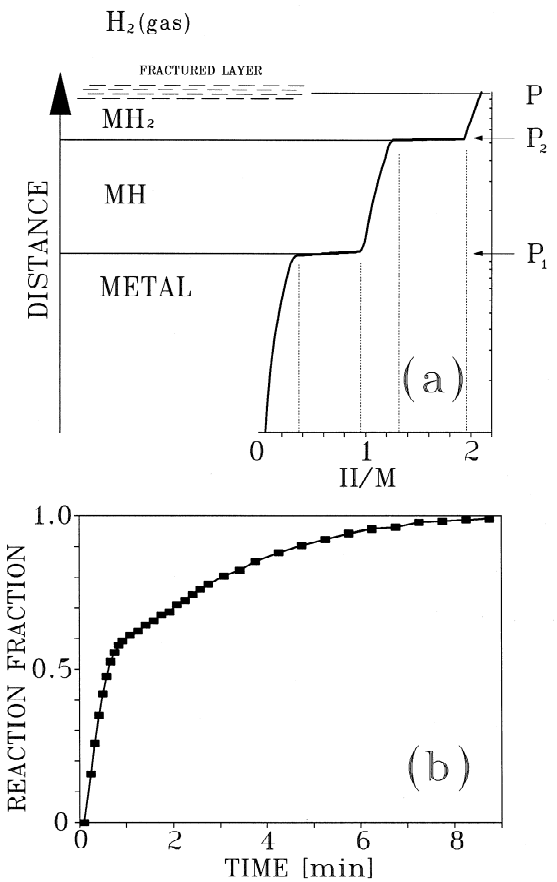

Fig. 5. (a) A schematic description of the structure [left side of (a)] and composition [right side of (a)] of the product-moving layer constructed on a metal forming mono- and di-hydrides under the working pressure *P*. P_1 and P_2 are the equilibrium (plateau) pressures for the mono- and di-hydrides, respectively; (b) Hydriding kinetics of titanium metal at 600 °C under 0.1 MPa H_2, demonstrating the separate formation of the β-phase and the dihydride, consecutively.

successively. In each layer a concentration gradient of the hydrogen is built, with limiting values governed by the appropriate isotherms. Evidently, for M–H systems for which only one hydride phase is formed (e.g. uranium), the layer consists of one type of hydride. The external product layer is often cracked, even for a relatively small density difference between the hydride and a ductile parent metal. The relative thickness of the layers and their hydrogen concentration gradients may change as the 'envelope' starts to contract. In particular, the higher hydride phase formation may be retarded. Upon achieving a steady-state condition the structure of the product-moving layer is retained through most of the remaining reaction. Evidently, to achieve steady-state conditions, samples are required with thicknesses which are much larger than the thickness of the product layer.

An actual example demonstrating the effect of the successive formation of two hydride phases during the same hydriding process on the kinetic behaviour is shown in Fig. 5b for hydriding of titanium metal [71]. The dissociation pressure of the hydrogen stabilized β-phase titanium at 600 °C is approximately 0.4 kPa ($P/P_{eq}=325$). The γ-phase hydride with composition TiH_2 and fcc fluorite-type structure [72,73] has a dissociation pressure of about 40 kPa ($P/P_{eq}=3.25$) [74]. Due to the extreme difference between the dissociation pressures, it is obvious that the β-phase transformation will be faster than the formation rate of the final γ-phase hydride. Thus, the fast initial stage is probably due to the transformation into the β-phase which can dissolve hydrogen up to a composition of TiH, about half of the reaction fraction. The second stage, the formation of the γ-phase hydride, is much slower. In fact, it may sometimes be altogether ignored [75]. It is operative only after completion of the β-phase transformation. For cases in which the dissociation pressures of both hydride phases are far below the working pressure, however, both phases may form almost simultaneously, moving together into the sample.

4.3. Determination of the hydride-front velocity

The overall kinetic curve, obtained for a given reacting system, is usually presented by the reacted fraction, $\alpha(t)$ dependence on reaction time, t. The overall kinetics can be measured using thermogravimetric, volumetric [19] or flow techniques. In fact, any measurable physical property which is sufficiently different for the metal compared with the hydride can serve to measure the absorption rate. Evaluating the IKPs (e.g. the hydride-front velocity, U_b), from the corresponding overall kinetic curve requires information concerning the morphology of the reacting sample, as well as the topochemistry of the hydride development [3]. The latter factor is determined using metallographic examinations of partially hydrided samples [64]. Once the topochemistry of the hydride progression has been identified (e.g. contracting envelope, preferred grain-boundary attack, etc.), the appropriate analysis procedure to evaluate the IKP can be utilized. It should be mentioned that some complex topochemical forms are rather difficult or even impossible to analyze. However, for contracting envelope-type morphology in samples of a well-defined geometry (a sphere, a wire, a foil or a parallelepiped of known dimensions), simple analytical functions link between $\alpha(t)$ and the hydride front displacement $X(t)=\int_0^t U_b(t)dt$. Using the front velocity $U_b=dX/dt$, examination of the X vs. time curve can show whether U_b is accelerated, decelerated or time independent. In the case of a constant (time-independent) bulk velocity, it may serve as an IKP. Constant-front velocities were observed for uranium [76,77], cerium [78], gadolinium [62,79] and zirconium [66,18]. On the other hand, bulk front velocities may be time dependent. Thus, for reactions controlled by diffusion through an adherent growing layer the velocity decelerates with time [3]. Such behaviour was found for the hydriding of thorium metal [80,81] and for a limited range of the reaction of uranium with deuterium [82] and for titanium [83].

4.4. Comparing the hydride-front velocity of uranium and thorium

Uranium and thorium are two hydride-forming metal actinides. Thorium reacts with hydrogen to give ThH_2 [84,85] and Th_4H_{15} [86]. The hydride-to-metal density ratio is 0.81 for the dihydride and 0.71 for the higher hydride. Under conditions when only the dihydride is stable, a protective hydride layer is formed over the thorium sample. The rate-determining step of the reaction is then the diffusion of the hydrogen through this growing hydride layer [80,81]. The overall hydriding kinetics thus obeys a parabolic-rate law. The front velocity is decelerating according to the expression $U_b(t)=k_{Th}t^{-1/2}$, where k_{Th} is a rate constant associated with the diffusion of hydrogen in the hydride. Uranium, on the other hand, produces a single, almost stoichiometric trihydride, UH_3 [87], with a hydride-to-metal density ratio of 0.57. This relatively large density change induces strain and cracking of the hydride which does not provide a protective adherent layer on the sample surface. Consequently, the hydride-front velocity is constant (time independent) [76,77], and the kinetics is controlled by the phase transformation occurring in the vicinity of the metal–hydride interface. The evaluated front displacements for these two actinides under 0.05 MPa H_2, at two different temperatures are compared in Fig. 6. The curves are plotted on a log–log scale. The different slopes, a unity for uranium, and 1/2 for thorium are evident.

This example demonstrates the possible effects of the physical properties of the hydride product and the parent metal on the hydriding mechanism.

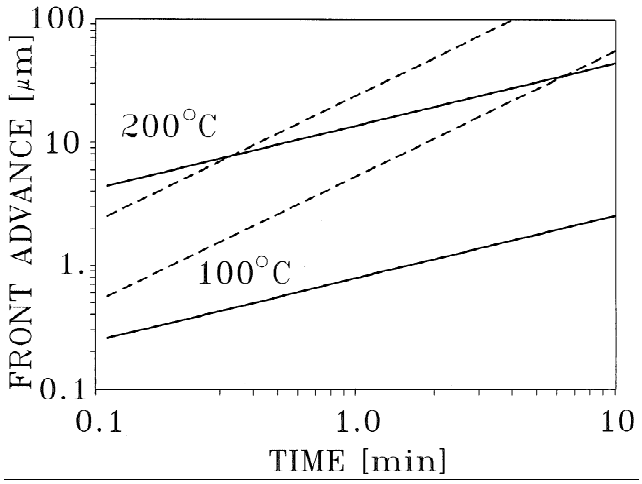

Fig. 6. A comparison of the evaluated kinetic behaviour of the hydride front advances in uranium (– – –) and thorium (———) under 0.05 MPa H_2, at two different temperatures. The data has been evaluated based on [98,80].

4.5. Deducing rate-controlling mechanisms from the hydride front-velocity behaviour

As mentioned above, U_b may be either constant or time-dependent. Obviously, a decelerating front velocity can be attributed to a diffusion-controlled rate-limiting step, as demonstrated in Section 4.3. For a time-independent (constant) front velocity, however, the rate-limiting process may be located at each of several possibilities [3]:

1. A surface-related process (such as dissociation, surface penetration, etc.) for a non-adherent hydride film with an effective constant thickness.
2. A transport (diffusion-controlled) process through a protective hydride film, with an effective constant thickness, as described in Section 4.3, or through a protective *internal* hydride film with an effective constant thickness, as described in Section 4.1 (the monohydride layer in Fig. 5a).
3. An interface-related process at either the metal–hydride, or the higher–lower hydride phases (Fig. 5a). The interface-controlled process may be either the injection of hydrogen atoms through the interface barrier or the solid-state phase transformation.

The identification of the rate-limiting step which is a main objective of the hydriding mechanism research, is thus not unique and more experimental factors must be considered. There are two general ways which may substantiate the validity of a specific mechanism:

1. A comprehensive analysis of the pressure–temperature dependence of the hydride-front velocity, and its comparison to model predictions [3].
2. Studying the effect of selected symptomatic physical–chemical and metallurgical properties of the reacting metal and its hydrides.

In the following sections we shall discuss these subjects.

4.6. The temperature and pressure dependence of the hydride-front velocity

Quite often, the temperature dependence of the constant hydride-front velocity, as well as other IKPs, for a given system obeys an Arrhenius law over a certain temperature range. However, deviations from a linear Arrhenius relation are apparent for temperature scans which are sufficiently wide. As a rule, such deviations are observed for relatively high temperatures, at which the reversible (decomposition) reaction is important. Quantitatively, this is found when the ratio of the applied to the equilibrium pressure approaches unity. We should note, in this context, that absorption equilibrium pressures are frequently higher than the corresponding decomposition pressures. This difference leads to the apparent hysteresis loops observed in the isotherms [88]. Approaching decomposition conditions causes the Arrhenius plots to level off, then drop rapidly with increasing temperature. This has been clearly observed for uranium metal [30,76,77,89] and for hafnium [90].

Besides the above effect of the reversible decomposition reaction, there have been some examples of deviations from a linear Arrhenius relation at a temperature range which is far below the decomposition temperature. Such deviations may be either due to a change in the controlling mechanism [91], or due to changes in the physical–mechanical properties of the reacting system. Thus, for zirconium, the apparent hydride-front velocity is decreased with temperature around 550 °C since the rate-limiting step is relocated to the β-phase formed above this temperature [67]. In titanium, the thickness of the non-adherent hydride layer is changing with reaction temperature causing deviations from a linear Arrhenius relation [83]. Deviations may arise also from the intrinsic behaviour of the given mechanism [92].

In Fig. 7 the Arrhenius plots for several metals and alloys are shown. It is interesting to note that the metals are grouped according to their chemical nature. Thus, the IVb group (Ti, Zr, Hf) is characterized by relatively high activation energies (around 100 kJ $mole^{-1}$ for all three metals [18,67,83,90]). For all three metals of this group, the basic hydriding mechanism was found to be controlled by diffusion of hydrogen through the product hydride layer. There were, of course, some modifications of the basic models, as mentioned above, for Ti [83] and for Zr [67]. However, the deviating parts of the temperature dependence were omitted from the figure, so that the primary similarity of the elements of this group compared with the other elements in the figure is clear.

The metals gadolinium and cerium represent the rare

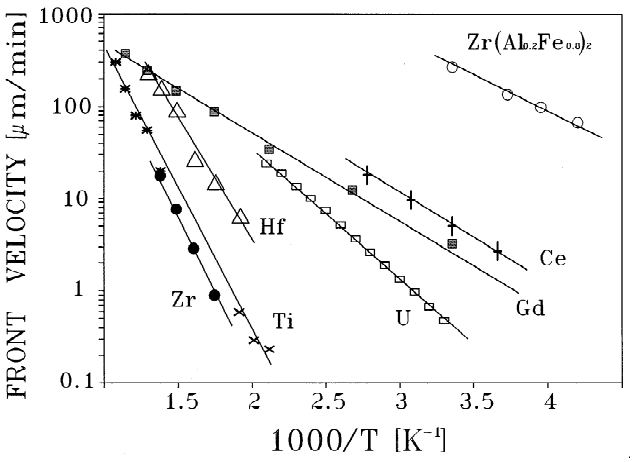

Fig. 7. Arrhenius plots of the hydride-front velocities for several metals and alloys under 0.1 MPa H_2. The data has been compiled based on references cited in Section 4.6. For titanium, the data was evaluated from two sources: (*) [75]; (×) [83].

earth elements. Here again, the apparent activation energies are similar, i.e. 20 kJ mole^{-1} for Ce [78], and 17 kJ mole^{-1} for gadolinium [79]. The hydride-front velocity for cerium is higher than that of gadolinium. This may reflect a general tendency of the light rare earths (i.e. La, Ce, Pr, Nd) having faster hydriding kinetics compared with the heavier lanthanides. The rate-determining step for these two metals is as yet unclear. Based on the pressure dependence of U_b, a surface-to-subsurface penetration has been suggested as the rate-controlling step for Ce [78]. Note that under similar P–T conditions, the absolute hydride-front velocity values are much higher for the rare earth metals compared with the group IVb metals. They are also higher than the velocities obtained for uranium. The apparent activation energies measured for uranium hydriding are around 30–40 kJ mole^{-1} [76,89,93,94]. The rate-limiting step for uranium was identified to be located at the metal–hydride interface (see Section 4.7).

The intermetallic compound $Zr(Al_{0.2}Fe_{0.8})_2$ is shown in Fig. 7, to demonstrate the large difference in the hydride-front velocities between intermetallics and pure metals. In contrast to the other curves in Fig. 7, obtained under 0.1 MPa H_2, this curve was obtained under 1 MPa H_2 [95]. However, the large difference can not be attributed to the pressure difference alone. There are indications that such high velocities characterize other intermetallics of the same group, i.e. $Zr(Al_xFe_{1-x})_2$ [96], as well as $LaNi_5$ [56], and $LaAl_{0.25}Ni_{4.75}$ [97]. Though the activation energies for these intermetallics are not much different than those of the rare earths, the absolute values of the hydride-front velocity are about two orders of magnitude higher. As discussed above (Section 4.1), the hydriding process in this case may involve a combination of cracking and nucleation. This may account for the relatively high effective hydride-front velocities in the intermetallic systems.

The pressure dependence of the hydride-front velocity has been effectively used to deduce the rate-limiting step in the massive stage of the hydriding process [1,3]. Thus, for example, the power– pressure dependence of approximately $P^{1/3}$ observed for cerium in the range 0.03–3 MPa [78], leads to the suggestion that the rate-limiting step in this case is the penetration of hydrogen from the surface into the subsurface region. However, in some cases, interpreting the pressure-dependence results should be considered cautiously. As stated above, the hydride-front velocity is very sensitive to changes in the hydrogen pressure near equilibrium, dropping abruptly as equilibrium is approached. On the other hand, at pressures much higher than the equilibrium pressure, the velocity may frequently become independent of hydrogen pressure. Such behaviour is characteristic of uranium [76,98,99] and of $LaNi_5$ [56]. For such a complex dependence, some quite elaborate models have been suggested [76,77,92,100–102]. These models can, in principle, account for a variety of possible pressure dependencies. Hence, additional evidence is required to substantiate the identification of the rate-limiting step.

4.7. Using some metal and hydride characteristics to identify the rate-limiting step

When the rate-limiting step is located at the metal–hydride interface, it is expected that the hydride-front velocity will be more sensitive to the structure, composition and/or other metallurgical–physical properties of the parent metal (or alloy). For a rate-limiting step which is not associated with that interface (see Section 4.5), a lower susceptibility to the metal properties is expected. This argument is not limited only to the hydriding mechanism but is also relevant to other gas–solid reactions as well. A well-known gas–solid reaction is the oxidation of silicon. The mechanism of the thermal oxidation of silicon is controlled by a combination of diffusion of the oxidizing species and a reaction at the Si–oxide interface [103]. It has been shown that the oxidation kinetics are a function of the crystallographic orientation of the silicon surface [104,105]. Only the linear rate constant, which is related to the interface-controlled reaction, was found to be orientation dependent, whereas the diffusion-related rate constant was independent of silicon crystal orientation. Similarly, for the uranium hydriding reaction a strong correlation has been observed between the hydride-front velocity and the metal structure [30,101], composition [30,106] and other properties such as microstrains [106]. In Fig. 8, the temperature dependence (in the form of Arrhenius plots) of the hydride-front velocity is shown for three uranium samples. Pure cold-worked uranium sample with banded structure yields curve Fig. 8a. Similarly, pure uranium samples, annealed above 700 °C and characterized by well-defined large grains, shown in curve Fig. 8b demonstrate considerably higher velocities. For the β-quenched U–0.1 wt% Cr shown in curve Fig. 8c, velocities almost two

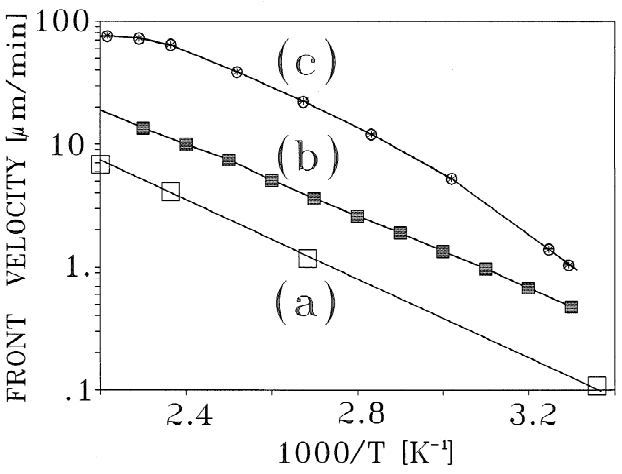

Fig. 8. The temperature dependence of the hydride-front velocities under 0.1 MPa H_2, (a) for pure cold-worked uranium sample with banded structure yields curve [76]; (b) pure uranium sample, annealed above 700 °C with well-defined large grains [98]; (c) β-quenched U–0.1 wt% Cr alloy [106].

orders of magnitude faster than those of curve Fig. 8a are observed. This increase of the hydride-front velocity is attributed to microstrained α-phase uranium formed by the β-quenching process [106]. These results are direct evidence associating the rate-limiting step of uranium hydriding to an interface-controlled process. It should be noticed, however, that in spite of the large difference in the absolute values of the hydride-front velocities, the apparent activation energy is practically unchanged.

For the metals of the IVb group, on the other hand, the hydriding is controlled by diffusion of hydrogen through the product hydride layer. For this case, obviously, only indirect correlation is expected between the metal characteristics and the hydriding-front velocity. Fig. 9 compiles

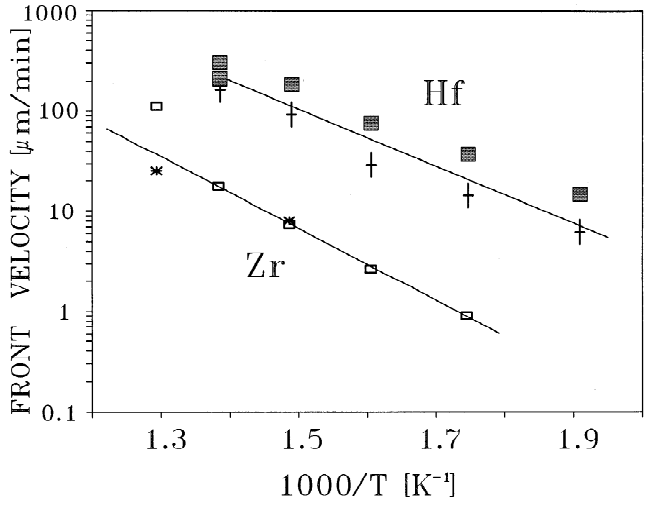

Fig. 9. The temperature dependence of the hydride-front velocity for zirconium [data points: □, Zircalloy from [18]; ×, pure zirconium from [67]] and hafnium [data depicted from [90]; +, crystal bar samples; ■, polycrystalline samples].

temperature dependence of the hydride-front velocity for zirconium and hafnium from several sources. It is clear that both pure zirconium and zircalloy (an alloy containing 1.55 wt% Sn and Cr, Fe and Ni in smaller amounts) have almost equal hydride-front velocities. This is in contrast to uranium in which 0.1 wt% Cr has a significant effect on the hydriding rate [30]. For hafnium, it seems that there is a difference between the crystal bar and the polycrystalline samples (see Fig. 9). However, this difference is much smaller than that observed for uranium having different microstructural characteristics (see Fig. 8). On the other hand, since the rate-limiting step for zirconium hydriding is the diffusion of hydrogen through the hydride product layer, then changing the hydride properties is expected to result in a change in the reaction kinetics. Indeed, as mentioned above, increasing the reaction temperature above the eutectoid temperature, leading to the formation of the β-phase, produces a change in the reaction kinetics. Since the diffusion through the β-phase is slower than that in the δ-hydride, the hydride-front velocity decreases at this temperature [67].

4.8. Comparing the surface and bulk hydride-front velocities

In Section 3.2 we discussed the surface nucleation rates and hydride nuclei growth velocities, U_s. In Section 4, the bulk velocity, U_b and its characteristics were considered. It was mentioned that U_s may be different to U_b under the same experimental conditions. Moreover, they may be associated with totally different mechanisms. For example, for uranium [50,60], cerium [58] and gadolinium [59] the surface front velocities are faster than the corresponding bulk velocities. For cerium, the activation energy for U_s, obtained from the Arrhenius plot, is different to that of U_b [58]. For uranium and gadolinium there is also a change in the behaviour of the Arrhenius plots of U_s and U_b, with the former indicating a change in slope occurring at the lower temperature region, which probably points to a change of the mechanism for U_s. All these differences are probably related to the different properties of the surface and the bulk such as transport properties or stress relief during the hydride growth. Yet, since the research of surface-front velocities is still preliminary, the meaning of these differences requires more effort. However, there is an important implication of the U_s/U_b velocity ratio for the topochemistry of the hydriding reaction. For $U_s/U_b \geq 1$, the stage when a complete overlapping of the spreading hydride nuclei is attained is characterized by a relatively thin layer, leading to an explicit contracting envelope morphology. For $U_s/U_b < 1$, on the other hand, the hydride nuclei starting on the sample surface tend to penetrate into the bulk in the form of hemispherical pits. A factor inhibiting fast surface velocity may be, for example, an improved SPL. Since such factors usually also affect the nucleation rate, the topochemistry in this case is a ‘pitting like attack’.

Moreover, in such a pitting attack, there is a higher probability of the hydride front advancing into the bulk along preferred paths, thus forming asymmetric hydride progress inside the bulk sample. It is obvious that such a pitting attack can not be analyzed according to the contracting envelope equations. Other measuring techniques should be used for such a case, preferentially based on direct observations.

5. Conclusions

In the present review, some recent results concerning the kinetics and mechanisms of the hydriding reactions in massive hydride-forming metals and alloys are briefly summarized.

Hydriding reactions involve a sequence of elementary steps, starting at the gas–surface region, continuing by some solid-state transport processes, and ending at the hydride-phase precipitation in the parent metal. The rate of the overall hydriding reaction may be determined by each of these steps, depending on the properties of the reacting systems, the experimental conditions and the stage of the reaction. According to the experimental results, the hydriding reaction is divided into three distinct successive stages, namely, the preliminary surface stages, the initial hydride nucleation and growth which may be accompanied by cracking, and the following main massive hydriding.

The following main conclusions, regarding the different stages of the reaction, can be summarized:

1. A wide variety of factors can affect the ability of the hydrogen gas molecules to cross the SPL and reach the solid metal. These include:
   (i) Modifications of the solid surface structure and composition using mechanical milling, chemical or heat treatments, and ion implantations.
   (ii) Deliberately changing the thickness of the SPL or depositing different material on top of the SPL.
   (iii) 'Poisoning' the gas phase with oxidizing impurities. The characteristics of the hydride nucleation at the early reaction stages are drastically influenced by the adsorption and transport properties of the SPL. Hence, the above modifications drastically affect the subsequent hydride nucleation rate.
2. Preheating activation is a necessary process preceding any kinetic measurement. Two different types of effects are attributed to this activation process: At low temperatures, desorption of certain functional groups (e.g. hydroxyls), which probably block hydrogen chemisorption sites, is induced (as found for uranium and the rare earth metals). At relatively high temperatures, the activation is associated with dissolution of the SPL into the metal, affecting the transport of hydrogen through the surface (as found for the IV group metals).
3. For brittle intermetallic compounds, early particulation may occur, making the direct probing of the surface nucleation and growth quite difficult.
4. The surface nucleation and growth rates of hydrides is a complex phenomenon. In some cases it involves more than one type (or 'a family') of nuclei, which differ in their characteristic nucleation rates and growth velocities. For uranium and gadolinium under certain experimental conditions, two types (at least) of such groups were identified.
5. The function describing the nucleation rate, dN/dt, has a defined maximum. A finite number, N_0, of preferred nucleation sites is available for each group of nuclei.
6. The growth process of hydride nuclei on the surface is, in many cases, quite isotropic (for polycrystalline materials). Hence, average surface growth velocity, U_s, may be evaluated under given $P–T$ conditions.
7. For the main massive hydriding stage, which follows the initial nucleation and growth, different topochemical forms of the hydride phase progression were identified. These forms include:
   (i) Contracting envelope (or shrinking core) morphology.
   (ii) Early particulation.
   (iii) Preferred grain boundary and edge attacks.The specific topochemical forms are determined by the type of system and by the experimental (e.g. $T–P$) conditions. Examples for the change in topochemistry are demonstrated by Zr and some rare earth metals which convert from a contracting envelope morphology into a preferred grain boundary attack as the reaction temperature is increased.
8. In multi-hydride systems (e.g. Ti) the contracting envelope is initially constructed of the lower hydride, and later, the higher hydride is formed on top of it. In most cases, the outer product layer is fractured.
9. Most of the rigorous kinetic studies involve contracting envelope progression of the hydride product layer on samples with well-defined geometrical shapes. The measured overall kinetic curves then provide exact evaluation of the IKPs. The $P–T$ dependence of the IKPs may point to a possible controlling mechanism.
10. The velocity of the hydride product layer, U_b, can be obtained for any contracting envelope morphology. For a rate-controlling transport of hydrogen through a thickening product layer (e.g. thorium), U_b is time dependent (proportional to $t^{-1/2}$).
11. U_b is constant during the massive reaction stage, under steady-state conditions. The rate-controlling step in this case may be located at the metal–hydride interface, the low- and high-hydride interface, the product layer surface or as a transport process through a product layer with an effectively constant thickness.
12. The apparent activation energies for U_b are correlated with the chemical nature of the reacting metal. Thus, for the group IV elements (Ti, Zr, Hf), apparent activation energies of about 100 kJ mole^{-1} were found, and for

the rare earth metals Ce and Gd, values of about 20 kJ mole^{-1} were obtained. This is probably related to the similar hydriding mechanisms characterizing the elements of the same chemical group (e.g., diffusion through the product layer for the group IV elements).

13. Assigning the rate-controlling mechanism can be substantiated by certain symptomatic trends. Thus, interface-controlled reactions are more susceptible to changes in the microstructure of the reacting metal (e.g., in uranium). Diffusion-controlled reactions are likely to depend on the nature and properties of the hydride formed.
14. The surface front velocities, U_s, are usually faster than the bulk product layer velocities, U_b (e.g. uranium, cerium, gadolinium). Evidently, the mechanism controlling the surface and bulk hydride-front advances are not identical. The differences between the surface and bulk velocities lead to different topochemical forms. Whereas for $U_s/U_b \geq 1$, an explicit contracting envelope morphology prevails, for $U_s/U_b < 1$ a 'pitting like attack' is observed.

Acknowledegments

The authors wish to thank Prof. I. Jacob for helpful discussions and Mr. M. Brill for assistance in the preparation of this work. The support of a joint grant from the Israel Council for Higher Education and Israel Atomic Energy Commision is acknowledged.

References

[1] T.B. Flanagan, in A.F. Andersen and A.J. Maeland (eds.), *Prc. Intl. Symp. on Hydrides for Energy Storage, 1977*, Pergamon, 1978, p. 135.
[2] P.S. Rudman, *J. Less-Common Metals, 89* (1983) 93.
[3] M.H. Mintz and J. Bloch, *Prog. Solid State Chem., 16* (1985) 163.
[4] For a recent review see Chap. 2, in L. Schlapbach (ed.), Hydrogen in Intermetallic Compounds II, *Topics Appl. Phy., 67*, Springer-Verlag, 1992, p. 15; see also, G. Alefeld and J. Volkl (eds.), Hydrogen in Metals I, *Topics Appl. Phy., 28*, Springer-Verlag, 1970, p. 321.
[5] F.P. Netzer and E. Bertel, Adsorption and catalysis on rare-earth surfaces, in K.A. Geschneidner and L. Eyring (eds.), *Handbook on the Physics and Chemistry of Rare Earths*, Vol. 5, North Holland, 1982, p. 217; F.P. Netzer and J.A. Matthew, *Rep. Prog. Phys., 49* (1986) 621.
[6] H.C. Siegman, L. Schlapbach and C.R. Brundle, *Phys. Rev. Lett., 40* (1978) 972.
[7] M. El-Batanouny, M. Strongin, G.P. Williams and J. Colbert, *Phys. Rev. Lett., 46* (1981) 269.
[8] D.E. Azofeifa and N. Clark, *Z. Phys. Chem., 181* (1993) 387.
[9] A. Krozer and B. Kasemo, *J. Less-Common Metals, 160* (1990) 323.
[10] G. Kuus and W. Martens, *J. Less-Common Metals, 75* (1980) 111.
[11] Y. Chen and J.S. Williams, *J. Alloys Comp., 217* (1995) 181.
[12] L. Zaluski, A. Zaluska, P. Tessier, J.O. Strom-Olsen and R. Schulz, *J. Alloys Comp., 217* (1995) 295.
[13] F. Liu, G. Sandrock and S. Suda, *Z. Phys. Chem., 183* (1994) 163.
[14] X.L. Wang and S. Suda, *J. Alloys Comp., 227* (1995) 58.
[15] D. Crusset, F. Bernard, E. Sciora and N. Gerard, *J. Alloys Comp., 204* (1994) 71.
[16] E. Fromm, *Z. Phys. Chem. N.F., 147* (1986) 61.
[17] B. Kasemo and E. Tornqvist, *Appl. Surface Sci., 3* (1979) 307.
[18] K. Une, *J. Less-Common Metals, 57* (1978) 93.
[19] J.P. Blackledge, Chemistry of metal hydrides as related to their applications in nuclear technology, Chap. 5 in W.M. Mueller, J.P. Blackledge and G.G. Libowitz (eds.), *Metal Hydrides*, Academic Press, 1968, p. 119.
[20] M.C. Burell and N.R. Armstrong, *Surface Sci., 160* (1985) 235.
[21] L.W. Owen and R.A. Scudamore, *Corrosion Sci., 6* (1966) 461.
[22] A.J. Paul and P.M.A. Sherwood, *Surface and Interface Anal., 10* (1987) 238.
[23] E. Swissa, N. Shamir, M.H. Mintz and J. Bloch, *J. Nucl. Mater., 173* (1990) 87.
[24] J. Bloch, E. Swissa and M.H. Mintz, *Z. Phys Chem. N.F., 164* (1989) 1193.
[25] T. Smith, *Surface Sci., 38* (1973) 292.
[26] P.E. West and P.M. George, *J. Vac. Sci. Technol., A5* (1987) 1124.
[27] F. Meli, Z. Sheng, I. Vedel and L. Schlapbach, *Vacuum, 41* (1990) 1938.
[28] K. Ichimura, M. Matsuyama and K. Watanabe, *J. Vac. Sci. Technol., A5* (1987) 220.
[29] V.I. Mikheeva and M.E. Kost, *Dokl. Akad. Nauk. SSSR, 115* (1957) 100.
[30] J. Bloch and M.H. Mintz, *J. Less-Common Metals, 166* (1990) 241.
[31] S. Myhra, E.H. Kisi and E.M. Gray, *J. Alloys Comp., 224* (1995) 305.
[32] T. Hirata, *J. Less-Common Metals, 107* (1985) 23.
[33] J. Bloch, D. Brami, A. Kremner and M.H. Mintz, *J. Less-Common Metals, 139* (1988) 371.
[34] D. Bedere and P. Sans, *J. Less-Common Metals, 91* (1983) 33.
[35] H. Sakaguchi, T. Tsujimoto and G. Adachi, *J. Alloys Comp., 223* (1995) 122.
[36] G.D. Sandrock and P.D. Goodell, *J. Less-Common Metals, 104* (1984) 159.
[37] A.A. Bulbich, *J. Alloys Comp., 196* (1993) 29.
[38] N. Gerard, *J. Less-Common Metals, 131* (1987) 13.
[39] N. Gerard and S. Ono, Chap. 4 in L. Schlapbach (ed.), Hydrogen in Intermetallic Compounds II, *Topics Appl. Phy., 67*, Springer-Verlag, 1992, p. 165.
[40] P. Dantzer and E. Orgaz, *J. Less-Common Metals, 147* (1989) 27.
[41] P. Dantzer and E. Orgaz, *Z. Phys. Chem. N.F., 164* (1989) 1267.
[42] M.H. Mintz and Y. Zeiri, *J. Alloys Comp., 216* (1994) 159.
[43] E.H. Kisi, C.E. Buckley and E.M. Gray, *J. Alloys Comp., 185* (1992) 369.
[44] H.H. van Mal, Stability of ternary hydrides and some applications, *Thesis*, Technological University of Delft, May, 4, 1976; *Philips Res. Repts., Suppl., No. 1* (1976) 22.
[45] T. Misawa and H. Sugawara, *J. Less-Common Metals, 89* (1983) 19.
[46] R. Choubey and M.P. Puls, *Metall. Mater. Trans., 25A* (1994) 993.
[47] G. Cannelli and R. Cantelli, *Mater. Sci. Eng., 47* (1981) 107.
[48] S.M. Lee and T.P. Perng, *J. Alloys Comp., 177* (1991) 107.
[49] Z. Haberman, M. Brill, M.H. Mintz, I. Jacob and J. Bloch, unpublished results.
[50] J. Bloch, F. Simca, M. Kroupp, A. Stern, D. Shmarjahu, M.H. Mintz and Z. Hadari, *J. Less-Common Metals, 103* (1984) 163.
[51] J.W. Christian, The theory of transformation in metals and alloys, Part 1, *Equilibrium and Kinetic Theory*, Pergamon Press, 1975.
[52] D.A. Young, *Decomposition of Solids*, Pergamon Press, 1966.
[53] L. Belkbir, E. Joly, N. Gerard, A. Percheron-Guegan and J.C. Achard, *J. Less-Common Metals, 73* (1980) 69.
[54] J.W. Larsen and B.R. Livesay, *J. Less-Common Metals, 73* (1980) 79.
[55] G.H. Kim, C.H. Chun, S.G. Lee and J.Y. Lee, *Acta Metall. Mater., 42* (1994) 3157.

[56] A. Osovizki, J. Bloch, M.H. Mintz and I. Jacob, *J. Alloys Comp*., *248* (1997) 209.
[57] A. Raveh, R. Arkush, S. Zalkind and M. Brill, *Surface Coatings Technol*., *82* (1996) 38.
[58] M. Brill, J. Bloch, D. Shmariahu and M.H. Mintz, *J. Alloys Comp*., *231* (1995) 368.
[59] M. Brill, M. Matiash, I. Jacob, M.H. Mintz and J. Bloch, unpublished results.
[60] M. Brill, M.H. Mintz and J. Bloch, in press.
[61] R. Arkush, A. Venkert, M. Aizenshtein, S. Zalkind, D. Moreno, M. Brill, M.H. Mintz and N. Shamir, *J. Alloys Comp*., *244* (1996) 197.
[62] J. Bloch, Kinetics and mechanisms of the hydridization of uranium and rare-earth metals, *Thesis submitted for the degree of Doctor of Philosophy, Ben-Gurin University of the Negev, Beer-Sheva, September 1983, NRCN-545*, Published by the Scientific and Technical Information Department, Nuclear Research Center–Negev, 1989.
[63] D. Moreno, S. Zalkind, R. Arkush and N. Shamir, *J. Nucl. Matter*., *230* (1996) 181.
[64] J. Bloch, Z. Hadari and M.H. Mintz, *J. Less-Common Metals, 102* (1984) 311.
[65] J. Bloch and M.H. Mintz, *J. Nucl. Matter., 110* (1982) 251.
[66] J. Bloch, I. Jacob and M.H. Mintz, *J. Alloys Comp., 191* (1993) 179.
[67] J. Bloch, *J. Alloys Comp., 216* (1994) 187.
[68] J. Paidassi and J. Nierlich, *C.R. Acad. Sci., Paris, 267* (1968) 1085.
[69] K. Dialer, *Monatsh. Chem., 79* (1948) 311.
[70] J.J. Reilly and G.D. Sandrock, *Scientific. Am., 242* (Feb. 1980) 98.
[71] Y. Levitin, M.H. Mintz and J. Bloch, unpublished results.
[72] G. Hägg, *Z. Phys. Chem., B11* (1931) 433.
[73] S.S. Sidhu, L. Heaton and D.D. Zauberis, *Acta Crystallogr., 9* (1956) 607.
[74] A.D. McQuillan, *Proc. Roy. Soc. (London) Ser. A, 204* (1950) 309.
[75] Y. Hirooka, M. Miyake and T. Sano, *J. Nucl. Mater., 96* (1981) 227.
[76] J. Bloch and M.H. Mintz, *J. Less-Common Metals, 81* (1981) 301.
[77] J.R. Kirkpatrick and J.B. Condon, *J. Less-Common Metals, 172–174* (1991) 124.
[78] D. Sarussi, I. Jacob, J. Bloch, N. Shamir and M.H Mintz, *J. Alloys Comp., 191* (1993) 91.
[79] M. Matiash, I. Jacob, M.H. Mintz and J. Bloch, unpublished results.
[80] D.T. Peterson and D.G. Westlake, *J. Phys. Chem., 63* (1959) 1514.
[81] D.T. Peterson and J. Rexer, *J. Less-Common Metals, 4* (1962) 92.
[82] R.M. Alire, B.A. Mueller, C.L. Peterson and J.R. Mosely, *J. Chem. Phys., 52* (1970) 37.
[83] A. Efron, Y. Lifshitz, I. Lewkowicz and M.H. Mintz, *J. Less-Common Metals, 153* (1989) 23.
[84] R.E. Rundle, C.G. Shull and E.O. Wollan, *Acta Crystallog., 5* (1952) 22.
[85] W.L. Korst, *Acta Crystallog., 15* (1962) 287.
[86] W.H. Zachariasen, *Acta Crystallog., 6* (1953) 393.
[87] R.E. Rundle, *J. Amer. Chem. Soc., 69* (1947) 1719.
[88] T.B. Flanagan and J.D. Clewly, *J. Less-Common Metals, 83* (1982) 127.
[89] W.M. Albrecht and M.W. Mallet, *J. Electrochem. Soc. 103* (1956) 404; W.M. Albrecht and M.W. Mallet, *J. Electrochem. Soc. 105* (1958) 610.
[90] Y. Levitin, J. Bloch and M.H. Mintz, *J. Less-Common Metals, 175* (1991) 219.
[91] M.H. Mintz, *J. Alloys Comp., 176* (1991) 77.
[92] M.H. Mintz and J. Bloch, *J. Chem. Phys., 78* (1983) 6569.
[93] H.J. Svec and F.R. Duke, *USAEC Report ISC-105*, 1950.
[94] E. Wicke and K. Otto, *Z. Phys. Chem. (Frankfurt), 31* (1962) 222.
[95] N. Bronfman, J. Bloch, M.H. Mintz, D. Sarussi and I. Jacob, *J. Alloys Comp., 177* (1991) 183.
[96] I. Jacob, N. Bronfman, M.H. Mintz and J. Bloch, *Z. Phys. Chem., 181* (1993) 289.
[97] Z. Haberman, J. Bloch, M.H. Mintz and I. Jacob, *J. Alloys Comp*., unpublished results.
[98] G.L. Powell, W.L. Harper and J.R. Kirkpatrick, *J. Less-Common Metals, 174* (1991) 116.
[99] G.L. Powell, R.N. Ceo, W.L. Harper and J.R. Kirkpatrick, *Z. Phys. Chem., 181* (1993) 275.
[100] J.B. Condon and E.A. Larsen, *J. Chem. Phys., 59* (1973) 855.
[101] J.B. Condon, *J. Phys. Chem., 79* (1975) 392.
[102] J.R. Kirkpatrick, *J. Phys. Chem., 85* (1981) 3444.
[103] B.E. Deal and A.S. Grove, *J. Appl. Phys., 36* (1965) 3770.
[104] J.R. Ligenza, *Phys. Chem., 65* (1961) 2011.
[105] B.E. Deal, *J. Electrochem. Soc., 125* (1978) 576.
[106] J. Bloch and M.H. Mintz, *J. Alloys Comp*., *241* (1996) 224.